Published in final edited form as:
J Biomech. 2013 July 26; 46(11): 1921–1927. doi:10.1016/j.jbiomech.2013.05.028.

Using regression models to determine the poroelastic properties of cartilage

Chen-Yuan Chung and **Joseph M. Mansour***
Department of Mechanical and Aerospace Engineering, Case Western Reserve University, 2123 Martin Luther King Jr. Drive, Cleveland, OH 44106, USA

Abstract

The feasibility of determining biphasic material properties using regression models was investigated. A transversely isotropic poroelastic finite element model of stress relaxation was developed and validated against known results. This model was then used to simulate load intensity for a wide range of material properties. Linear regression equations for load intensity as a function of the five independent material properties were then developed for nine time points (131, 205, 304, 390, 500, 619, 700, 800, and 1000 s) during relaxation. These equations illustrate the effect of individual material property on the stress in the time history. The equations at the first four time points, as well as one at a later time (five equations) could be solved for the five unknown material properties given computed values of the load intensity. Results showed that four of the five material properties could be estimated from the regression equations to within 9% of the values used in simulation if time points up to 1000 s are included in the set of equations. However, reasonable estimates of the out of plane Poisson's ratio could not be found. Although all regression equations depended on permeability, suggesting that true equilibrium was not realized at 1000 s of simulation, it was possible to estimate material properties to within 10% of the expected values using equations that included data up to 800 s. This suggests that credible estimates of most material properties can be obtained from tests that are not run to equilibrium, which is typically several thousand seconds.

Keywords

Stress relaxation; Poroelasticity; Transversely isotropic; Linear regression

1. Introduction

Mechanically, articular cartilage is often modeled as a two-phase material with solid and fluid phases. Parallel constitutive models have been proposed using either biphasic (Mow et al., 1980) or poroelastic (Simon et al., 1983) theories. Although these theories developed from different roots, the governing equations of linear biphasic theory are mathematically equivalent to those of Biot's theory (Biot, 1941) for linear quasi-static poroelasticity with incompressible constituents (Simon, 1992). Using these models, and tests such as confined or unconfined compression, constitutive constants can be determined by fitting analytical models to measured data (Armstrong et al., 1984; Bursać et al., 1999; Mow et al., 1980).

*Corresponding author. Tel.: +1 2163684190; fax: +1 2163683007. mansour@case.edu, jmm12@case.edu (J.M. Mansour).

Conflict of interest statement
The authors have no conflicts to disclose.

Typically, material properties are found using an optimization procedure that fits a model to experimental data (Lei and Szeri, 2007; Cao et al., 2006; Athanasiou et al., 1995).

The objective of this work is to investigate the feasibility of using regression models to determine the poroelastic properties of cartilage tested in unconfined compression. Such models could simplify the process for determining material properties from measured data.

2. Methods

An axisymmetric poroelastic model for unconfined compression stress relaxation was developed using ANSYS. In an unconfined compression stress relaxation test, a thin cylindrical specimen is compressed between two rigid impermeable and smooth platens while surrounded by fluid (Fig. 1).

For this investigation we used a transversely isotropic model that shows good agreement with unconfined compression measurements in growth plate (Cohen et al., 1998). The compliance matrix for transverse isotropy has five independent constants (Bower, 2009)

$$S_{ijkl}=\begin{bmatrix} \frac{1}{E_t} & -\frac{\nu_t}{E_t} & -\frac{\nu_{at}}{E_a} & 0 & 0 & 0 \\ -\frac{\nu_t}{E_t} & \frac{1}{E_t} & -\frac{\nu_{at}}{E_a} & 0 & 0 & 0 \\ -\frac{\nu_{at}}{E_a} & -\frac{\nu_{at}}{E_a} & \frac{1}{E_a} & 0 & 0 & 0 \\ 0 & 0 & 0 & \frac{1}{\mu_a} & 0 & 0 \\ 0 & 0 & 0 & 0 & \frac{1}{\mu_a} & 0 \\ 0 & 0 & 0 & 0 & 0 & \frac{2(1+\nu_t)}{E_t} \end{bmatrix} \quad (1)$$

where E, ν, and μ are Young's modulus, Poisson's ratio, and shear modulus, respectively. The subscripts t and a indicate the transverse and axial or out-of-plane directions.

Cartilage was modeled using the coupled pore-pressure element CPT213, which is based on Biot's poroelasticity theory (ANSYS, 2010). This element is a fully direct coupling in which the mechanical equilibrium and fluid continuity equations are satisfied simultaneously. The axis of symmetry coincided with the global Y-axis in ANSYS. The directions of X, Y and Z were radial, axial and circumferential, respectively. The stress in the Y direction in ANSYS represents the effective stress in the Z direction in Armstrong et al. (1984). The total compressive stress is equal to the fluid pressure subtracted from the effective stress, i.e., $\sigma_a^t=\sigma_a^e-p_0$. Using ANSYS, transverse isotropy is modeled as a special case of orthotropic isotropy. Although nine elastic constants are needed to model orthotropic isotropy, only five independent constants are needed for transverse isotropy.

We applied the boundary conditions used by Cohen et al. (1998): the displacement imposed on the specimen was linear over time, reached its maximum value of 10% of the cartilage thickness at t_0 = 131 s. It was then held constant for 869 s. Axial displacement was constrained on the bottom of the specimen. Free fluid flow was enabled across the lateral boundaries. In contrast, the fluid was not permitted across the boundaries with the upper and lower platens.

The computational model was validated using data and results in Cohen et al. (1998). The specimen was a cylinder with radius a = 3.175 mm and thickness h = 1 mm. The five independent elastic constants were Young's moduli in the transverse plane E_t = 4.3MPa and out of plane E_a = 0.64MPa, Poisson's ratios in the transverse plane ν_t = 0.49 and out of plane ν_{at} = 0 and the out-of-plane shear modulus, μ_a, which could be any value for the case of uniaxial loading. Permeability was assumed to be the same in both the axial and transverse directions: $k = 5 \times 10^{-15}$ m^4 N^{-1} s^{-1}. Based on the assumption that, for a soft tissue the solid

and fluid phases are incompressible, the Biot coefficient equals one, and the reciprocal of the Biot modulus is zero (Simon, 1992). Load intensity at each time was computed by dividing the total force on the top surface of the model by its undeformed area. Nonlinear static analysis was performed using the Newton-Raphson algorithm with an unsymmetric option. A macro, written in the ANSYS parametric design language, performed the procedure automatically.

The load intensity (f) was computed at nine time points during relaxation: 131 s (when the ramp displacement reached the maximum) and 205, 304, 390, 500, 619, 700, 800 and 1000 s. These points were chosen from among the time points in Cohen et al. (1998). Simulations were performed using a range of material properties of growth plate (Villemure and Stokes, 2009) (Table 1). Two of the five properties were varied in each set of simulations, resulting in ten combinations of properties. Within each combination, simulations were performed for the range of material properties in Table 1. This process systematically populated the solution space for load intensity as a function of feasible material properties. Load intensity was normalized ($\bar{f}$) by the maximum value obtained from all simulations at a given time. Each material property was normalized by its largest value (Table 1).

Regression models were obtained by fitting the normalized load intensity to first-order polynomial equations in the normalized material properties at each time point, which resulted in nine equations. Any five of these equations can be solved using known values of the load intensity to obtain estimates of the five unknown material properties. In this investigation, known load intensity was obtained from simulated stress relaxation found using the best-fit material property data from Cohen et al. (1998). Material properties obtained from the regression equations and reverted to physical values (p_r) were compared with those used to validate our computational model (p_v). The error in the predicted properties was computed using error = $|(p_r - p_v)/p_v| \times 100\%$.

3. Results

Load intensity obtained from our finite element model is almost identical to that given by Cohen et al. (1998), which validates the computational model (Figs. 2 and 3). Although load intensity varied approximately linearly with material properties, there were regions with nonlinear behavior (Figs. 4–13). For example, load intensity at 1000 s deviated from linear behavior for E_t between 4.3 MPa and 6 MPa and for ν_t between 0.24 and 0.4 (Fig. 6b). Load intensity at 1000 s also deviated from linear behavior for E_t between 4.3 MPa and 6 MPa and for k between 1.8×10^{-15} m^4 N^{-1} s^{-1} and 3×10^{-15} m^4 N^{-1} s^{-1} (Fig. 8b).

Linear regression equations for the normalized load intensity at specific times (Eqs. (2)–(10)) showed good fits to the simulated data ($p < 0.001$ and $R^2 > 0.9$ for all equations). However, the coefficients of ν_{at} at 304, 390 and 500 s, shown in the equations below, were not significant ($p > 0.05$) and were set to zero when using the corresponding regression equations to determine mechanical properties.

$$\bar{f}_{131s} = 0.4874 + 0.2054\bar{E}_t + 0.2250\bar{E}_a + 0.1032\bar{\nu}_t - 0.0659\bar{\nu}_{at} - 0.3534\bar{k} \quad (2)$$

$$\bar{f}_{205s} = 0.9387 - 0.2107\bar{E}_t + 0.3950\bar{E}_a - 0.0756\bar{\nu}_t - 0.0422\bar{\nu}_{at} - 0.5852\bar{k} \quad (3)$$

$$\bar{f}_{304s} = 0.7281 - 0.1787\bar{E}_t + 0.5179\bar{E}_a - 0.1121\bar{\nu}_t - 0.0082\bar{\nu}_{at} - 0.4822\bar{k} \quad (4)$$

$$\bar{f}_{390s}=0.5227-0.1114\bar{E}_t+0.6175\bar{E}_a-0.0960\bar{\nu}_t+0.0030\bar{\nu}_{at}-0.3628\bar{k} \quad (5)$$

$$\bar{f}_{500s}=0.3277-0.0575\bar{E}_t+0.7298\bar{E}_a-0.0684\bar{\nu}_t+0.0081\bar{\nu}_{at}-0.2361\bar{k} \quad (6)$$

$$\bar{f}_{619s}=0.1927-0.0277\bar{E}_t+0.8250\bar{E}_a-0.0447\bar{\nu}_t+0.0094\bar{\nu}_{at}-0.1414\bar{k} \quad (7)$$

$$\bar{f}_{700s}=0.1332-0.0165\bar{E}_t+0.8733\bar{E}_a-0.0331\bar{\nu}_t+0.0095\bar{\nu}_{at}-0.0981\bar{k} \quad (8)$$

$$\bar{f}_{800s}=0.0840-0.0084\bar{E}_t+0.9167\bar{E}_a-0.0227\bar{\nu}_t+0.0093\bar{\nu}_{at}-0.0619\bar{k} \quad (9)$$

$$\bar{f}_{1000s}=0.0334-0.0011\bar{E}_t+0.9657\bar{E}_a-0.0108\bar{\nu}_t+0.0089\bar{\nu}_{at}-0.0245\bar{k} \quad (10)$$

These equations show the relative contribution of each of the five properties to the normalized load intensity during relaxation. At 131 s, when the displacement has come to equilibrium, permeability is dominant. At times greater than 131 s the relative influences of material properties vary. As time increases, the effect of the transverse Young's modulus diminishes while that of the axial Young's modulus increases to where it dominates the load intensity at 1000 s, which is in accordance with results given by Cohen et al. (1998), who showed that $f_{eq} = E_a\dot{\varepsilon}_0 t_0$. For times greater than 390 s the effect of the transverse Poisson's ratio decreases. The effect of the out-of-plane Poisson's ratio is generally small, but not zero, at all times, which suggests that assuming $\nu_{at} = 0$ as in Cohen et al. (1998) is inappropriate, as also noted by Bursać et al. (1999). The effect of permeability continually decreases with time, but does not go to zero. At 1000 s permeability is second only to axial Young's modulus in terms of effect on load intensity. In addition, the sign on each term indicates that a material property either increases or decreases the load intensity.

Solving subsets of five equations, chosen from Eqs. (2)–(10), with the coefficients of $\bar{\nu}_{at}$ in Eqs. (4)–(6) set to zero, showed that it was possible to get good estimates of the material properties used for validation. For example, solving the Eqs. (2)–(6), five normalized material properties were determined and converted to physical values. Comparing these five values with the input biphasic parameters used in ANSYS, the predicted errors of E_t, E_a, ν_t and k are 13.4%, 1.42%, 13.1%, and 2.03%, respectively. The value of ν_{at} was 0.0014, which was assumed to be zero by Cohen et al. (1998). Different combinations of equations produced differing values of the error, and out of plane Poisson's ratio that in most cases was negative (Table 2). The longer a simulation is run, the smaller the error in predicting material properties.

4. Discussion

We used a transversely isotropic model to map the solution space for load intensity in stress relaxation over a range of material properties that are expected to encompass those for growth plate. Regression equations fit to these results showed that it was possible to get credible estimates of the material properties of the model. A transversely isotropic model was used since it has been shown to produce good fits to experimental data for growth plate and chondroepiphysis. In contrast, this model does not provide as good a fit to stress relaxation data for articular cartilage (Bursać et al., 1999). It was not our intent to validate or suggest that a transversely isotropic model is a universal model for cartilage mechanics.

Transverse isotropy was used as an example of a reasonably good model with more parameters than a simple isotropic model. This model served the purpose of illustrating an approach for determining material properties using regression equations. However, the approach developed in this investigation could, in principle, be used to determine regression equations for finding material properties of a material model with any number of constants.

The values of material properties obtained from the regression equations depend on which set of five equations are used. We found that to get estimates that were closest to the expected values it was best to include time points where the stress was relaxing most rapidly plus at least one point where the stress was approaching a steady state.

Regression equations showed that the effect of permeability was the dominant contributor to load intensity at earlier times but its effect diminished as time increased. However, permeability remained second only to axial Young's modulus in contributing to the computed load intensity at 1000 s, which suggests that at 1000 s a sample may not have reached equilibrium. This is consistent with common practice where tests are run for several thousand seconds (Armstrong et al., 1984; Bursać et al., 1999; Mow et al., 1980). A potentially valuable result of this investigation is prediction of material properties without the need to run a test for long times (Table 2). Errors of less than 10% are incurred by stopping a test at 800 s. If only E_a and k are of interest, then reasonable estimates can be obtained from tests that do not exceed 500 s. Reducing the time to complete a test to 500 s from several thousand can be significant, particularly when a large number of samples need to be evaluated.

Negative values for the out of plane Poisson's ratio are, in principle, possible (Lakes, 1991; Naili et al., 1998). However, negative values predicted by the regression equations are outside of the range used in simulations, and therefore cannot be accepted as reasonable estimates of this property. Although negative, values of ν_{at} were close to zero as assumed by Cohen et al. (1998). A further limitation of this approach is that regression equations can only be applied to data from a test with the same boundary conditions as the finite element model. It is also possible that actual material properties may be outside of the ranges used to establish the regression equations, however, the range of material properties used in simulations could be expanded or focused on particular ranges. Since tissue engineered cartilage is often more compliant than native cartilage, regression equations could be developed for lower ranges of E_a and other material properties.

In summary, we have shown the feasibility of determining four poroelastic material properties from the solution of simple linear algebraic equations, and that it may not be necessary to run tests to equilibrium to obtain credible estimates of material properties.

Acknowledgments

This work was funded by the National Institutes of Health (Grant number P01 AR053622). The content is solely the responsibility of the authors and does not necessarily represent the official views of the National Institutes of Health.

References

ANSYS. ANSYS mechanical APDL and mechanical aaplications theory reference, Release 13.0. Canonsburg, PA, USA: ANSYS Inc.; 2010.

Armstrong CG, Lai WM, Mow VC. An analysis of the unconfined compression of articular cartilage. Journal of Biomechanical Engineering. 1984; 106:165–173. [PubMed: 6738022]

Athanasiou KA, Agarwal A, Muffoletto A, Dzida FJ, Constantinides G, Clem M. Biomechanical properties of hip cartilge in experimental animal models. Clinical Orthopaedics and Related Research. 1995; 316:254–266. [PubMed: 7634715]

Biot MA. Gerneral theory of three-dimensional consolidation. Journal of Applied Physics. 1941; 12:155–164.

Bower, AF. Applied Mechanics of Solids. Boca Raton, Florida: CRC Press; 2009.

Bursać PM, Obitz Toby W, Eisenberg Solomon R, Stamenović Dimitrije. Confined and unconfined stress relaxation of cartilage: appropriateness of a transversely isotropic analysis. Journal of Biomechanics. 1999; 32:1125–1130. [PubMed: 10476852]

Cao, Li; Youn, Inchan; Guilak, Farshid; Setton, Lori A. Compressive properties of mouse articular cartilage determined in a novel micro-indentation test method and biphasic finite element model. Journal of Biomechanical Engineering. 2006; 128:766–771. [PubMed: 16995764]

Cohen B, Lai WM, Mow VC. A transversely isotropic biphasic model for unconfined compression of growth plate and chondroepiphysis. Journal of Biomechanical Engineering. 1998; 120:491–496. [PubMed: 10412420]

Lakes R. Deformation mechanisms in negative Poisson's ratio materials: structural aspects. Journal of Materials Science. 1991; 26:2287–2292.

Lei, Fulin; Szeri, AZ. Inverse analysis of constitutive models: biological soft tissues. Journal of Biomechanics. 2007; 40:936–940. [PubMed: 16730739]

Mow VC, Kuei SC, Lai WM, Armstrong CG. Biphasic creep and stress relaxation of articular cartilage in compression: theory and experiments. Journal of Biomechanical Engineering. 1980; 102:73–84. [PubMed: 7382457]

Naili S, Oddou C, Geiger D. A method for the determination of mechanical parameters in a porous elastically deformable medium: applications to biological soft tissues. International Journal of Solids and Structures. 1998; 35:4963–4979.

Simon BR. Multiphase poroelastic finite element models for soft tissue structures. Applied Mechanics Reviews. 1992; 45:191–218.

Simon, BR.; Wu, JSS.; Evans, JH. Poroelastic mechanical models for the intervertebral disc. In: Bartel, DL., editor. Proceedings of Advances in Bioengineering; ASME Winter Annual Meeting; 13–18 November; Boston, MA, USA. 1983. p. 106-107.

Villemure I, Stokes IAF. Growth plate mechanics and mechanobiology. A survey of present understanding. Journal of Biomechanics. 2009; 42:1793–1803. [PubMed: 19540500]

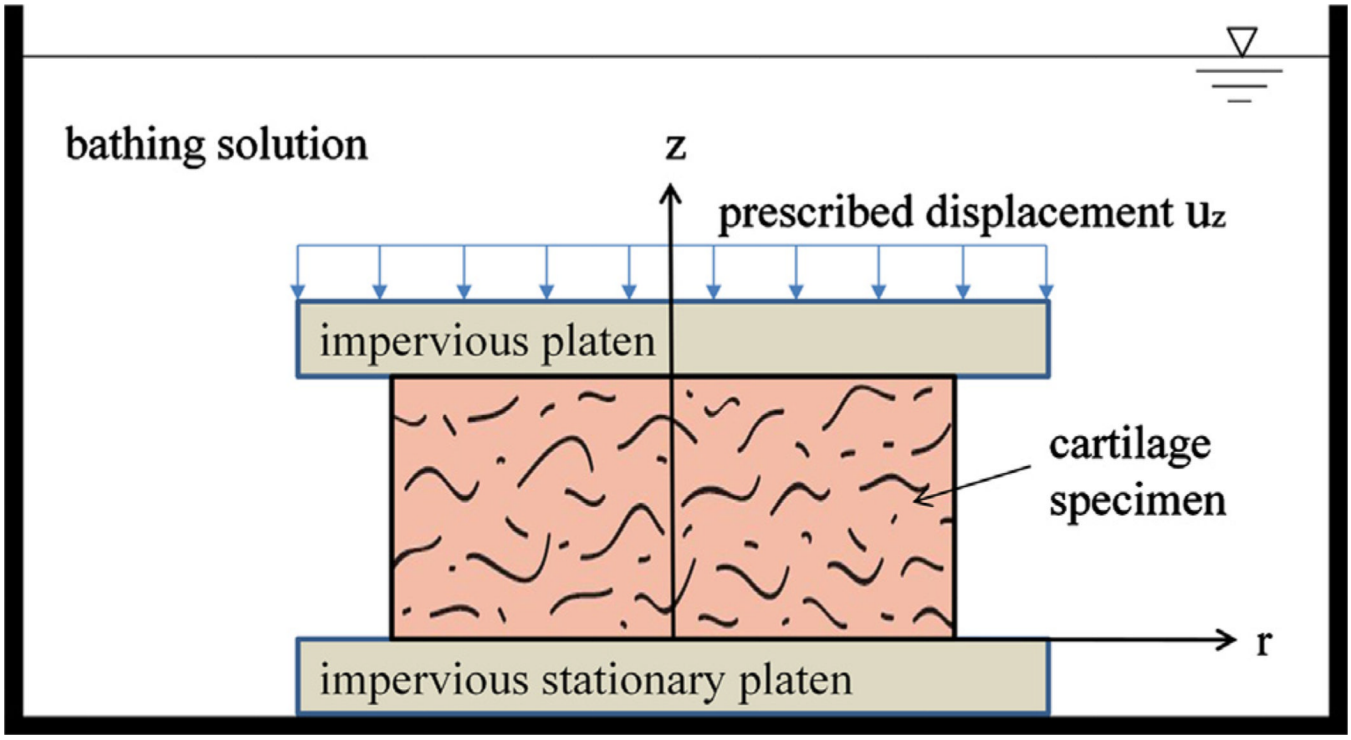

Fig. 1.

Schematic of the unconfined compression test of a cylindrical disk of hydrated cartilage. The same boundary conditions used in Cohen et al. (1998), were applied. The specimen was free to expand in the radial direction. Displacements in the axial direction were constrained on the bottom of the specimen in contact with the stationary platen. Free fluid flow was enabled across the lateral boundaries, i.e., fluid pressure was set as zero on the cylindrical periphery. In contrast, the fluid was not permitted across the boundaries with the upper and lower platens.

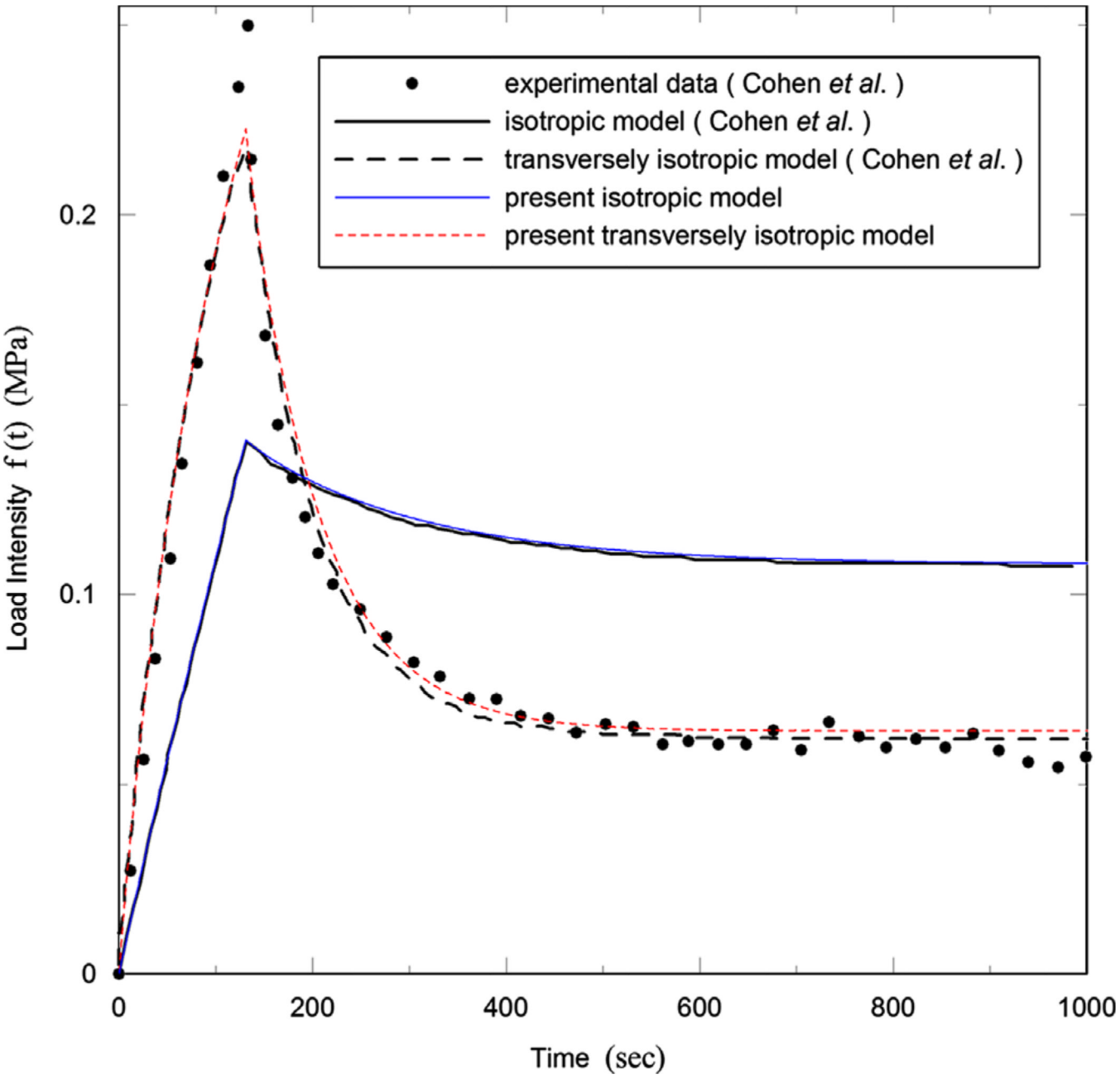

Fig. 2.

Comparison of the transversely isotropic and an isotropic model, both developed using ANSYS, and the analytical solution of those models and experimental results from Cohen et al. (1998). For the isotropic model, Young's modulus was $E = 1.08$ MPa, Poisson's ratio was $\nu = 0$, and permeability was $k = 15.5 \times 10^{-15}$ m^4 N^{-1} s^{-1}, which are the same values used in Cohen et al. (1998).

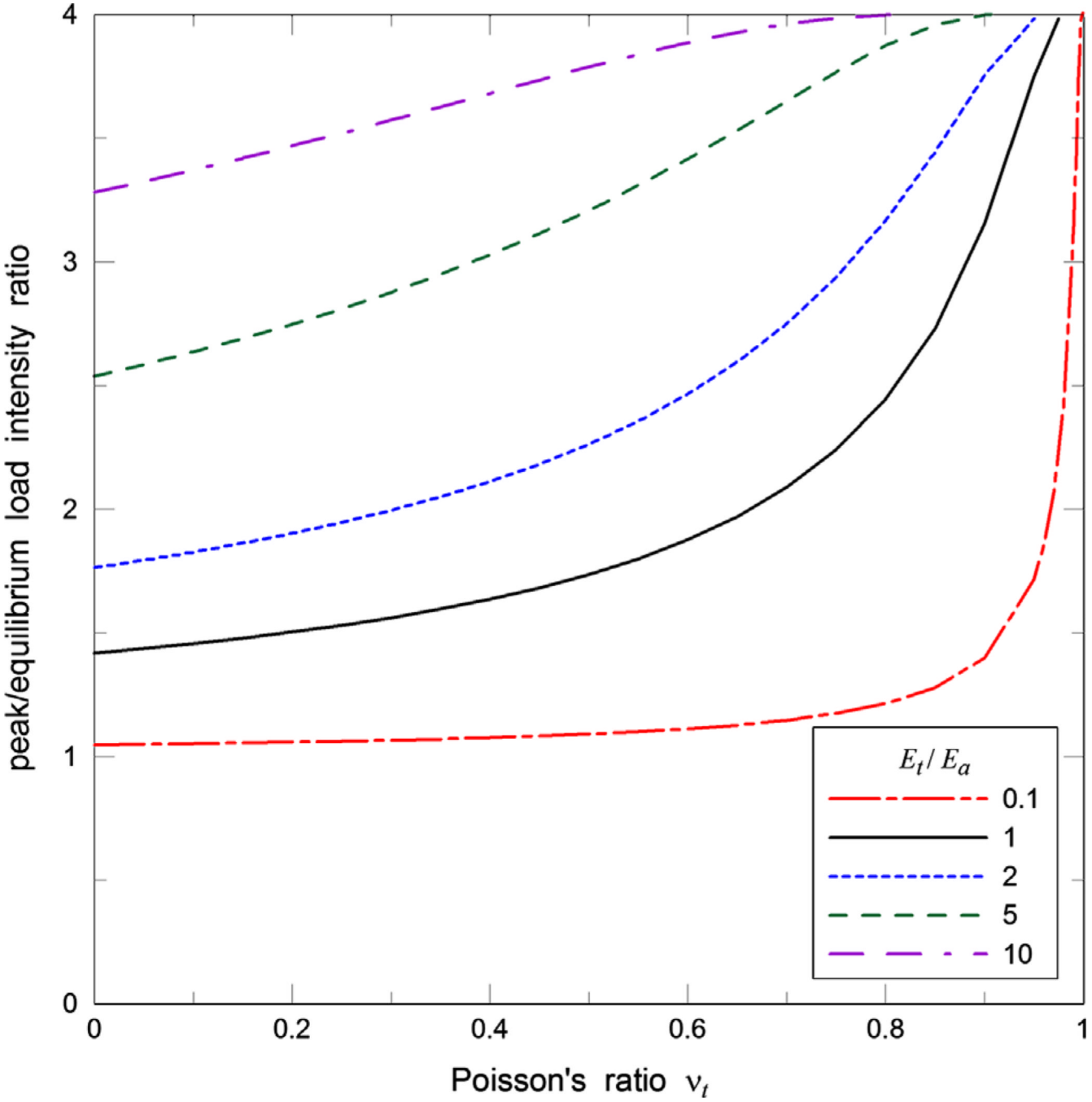

Fig. 3.

Parametric dependence of the ratio of the load intensity at peak to that at equilibrium for values of E_t/E_a between 0.1 and 10. All other material properties are the same as used in Fig. 2. It is important to note that the transversely isotropic model could provide a good fit without limiting f_{peak}/f_{eq} to 1.5, with the result that the experimental measured peak stress will not be underestimated (Bursać et al., 1999).

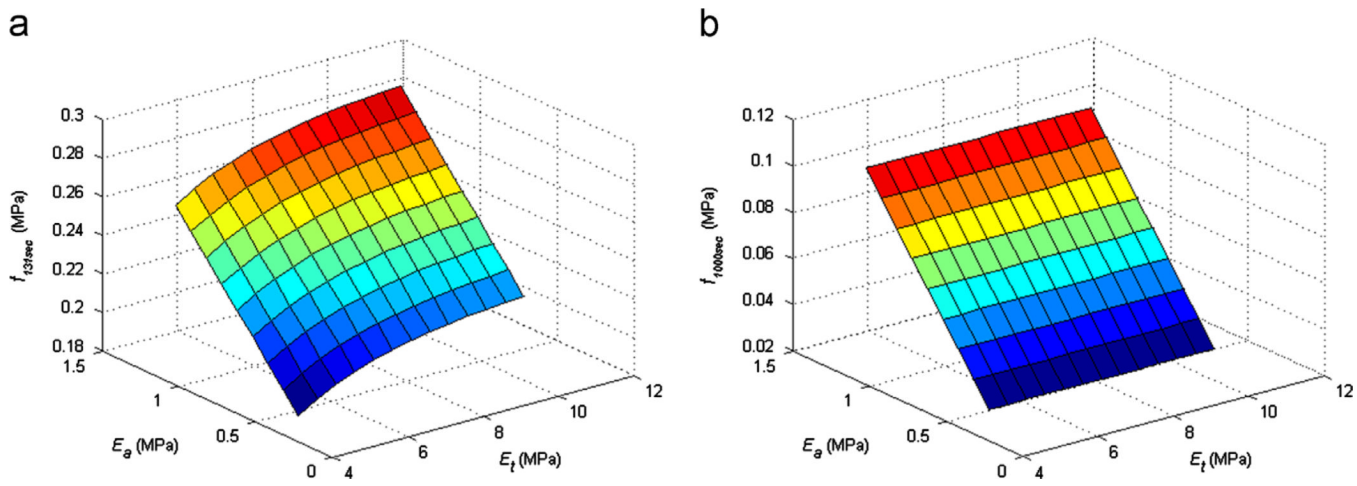

Fig. 4.

Plots of load intensity at (a) 131 s and (b) 1000 s as a function of Young's modulus in plane and out of plane where $\nu_t = 0.49$, $\nu_{at} = 0$ and $k = 5 \times 10^{-15}$ m^4 N^{-1} s^{-1}.

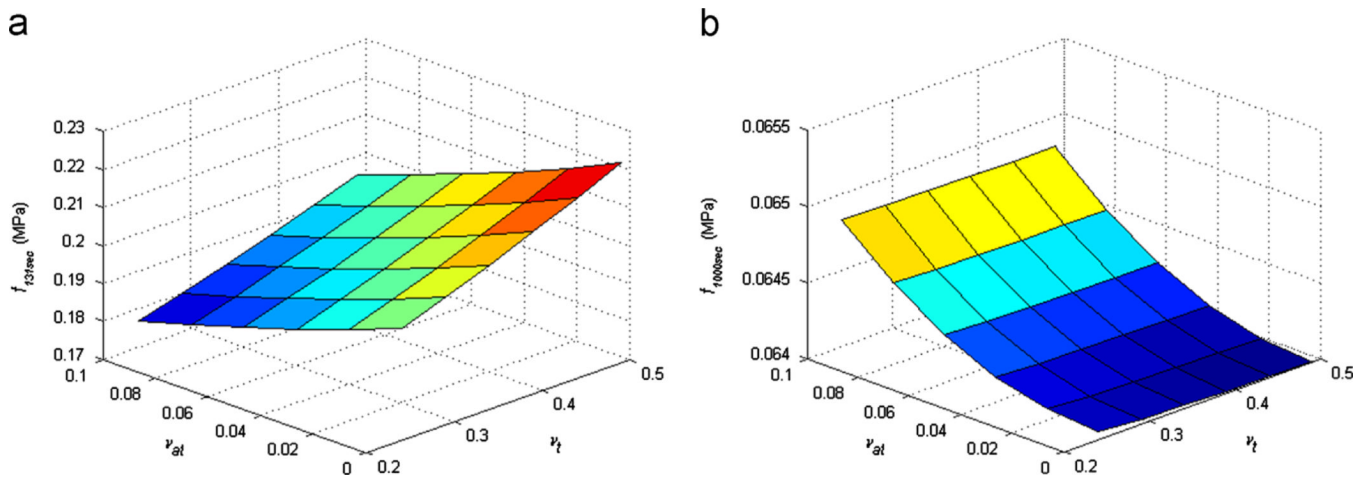

Fig. 5.

Plots of load intensity at (a) 131 sec and (b) 1000 sec as a function of Poisson's ratio in plane and out of plane where $E_t = 4.3$ MPa, $E_a = 0.64$ MPa and $k = 5 \times 10^{-15}$ m^4 N^{-1} s^{-1}.

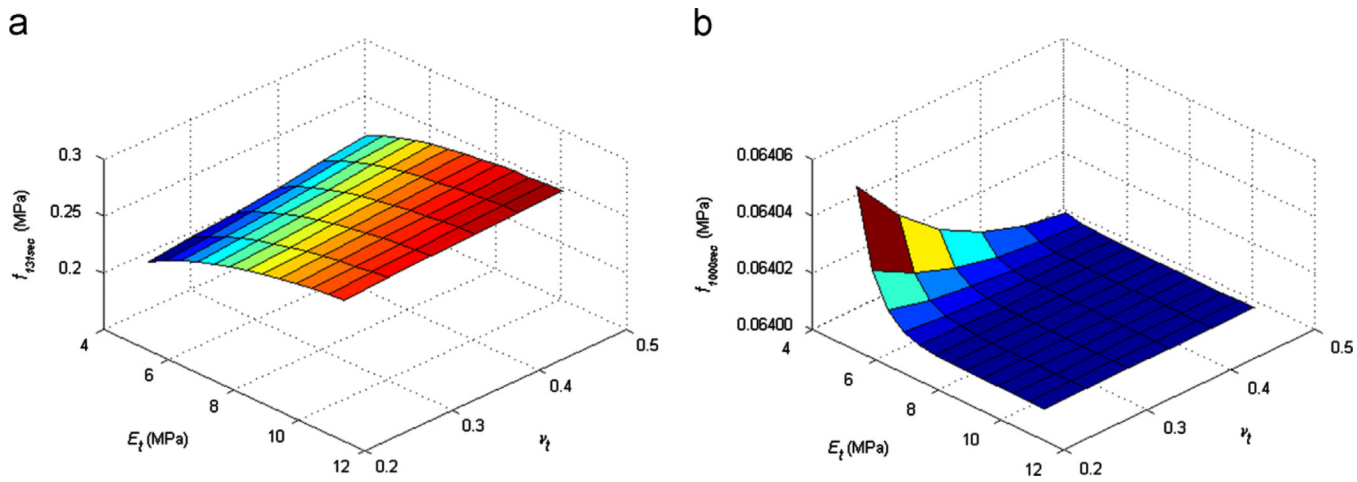

Fig. 6.

Plots of load intensity at (a) 131 s and (b) 1000 s as a function of Poisson's ratio in plane and Young's modulus in plane where $E_a = 0.64$ MPa, $\nu_{at} = 0$ and $k = 5 \times 10^{-15}$ m^4 N^{-1} s^{-1}.

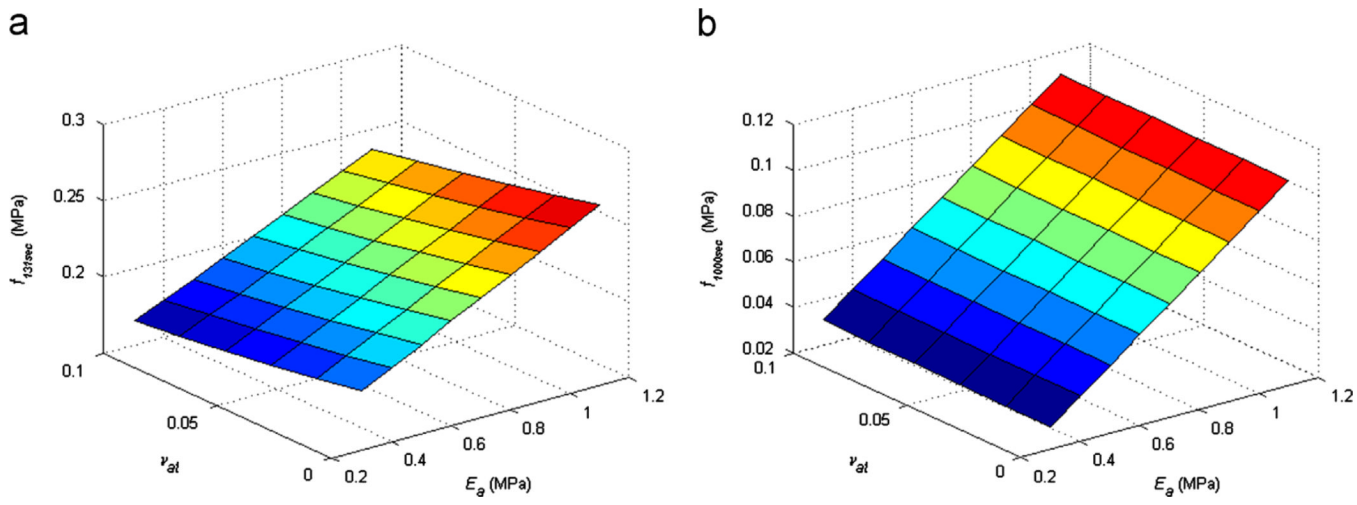

Fig. 7.

Plots of load intensity at (a) 131 s and (b) 1000 s as a function of Young's modulus out of plane and Poisson's ratio out of plane where $E_t = 4.3$ MPa, $\nu_t = 0.49$ and $k = 5 \times 10^{-15}$ m^4 N^{-1} s^{-1}.

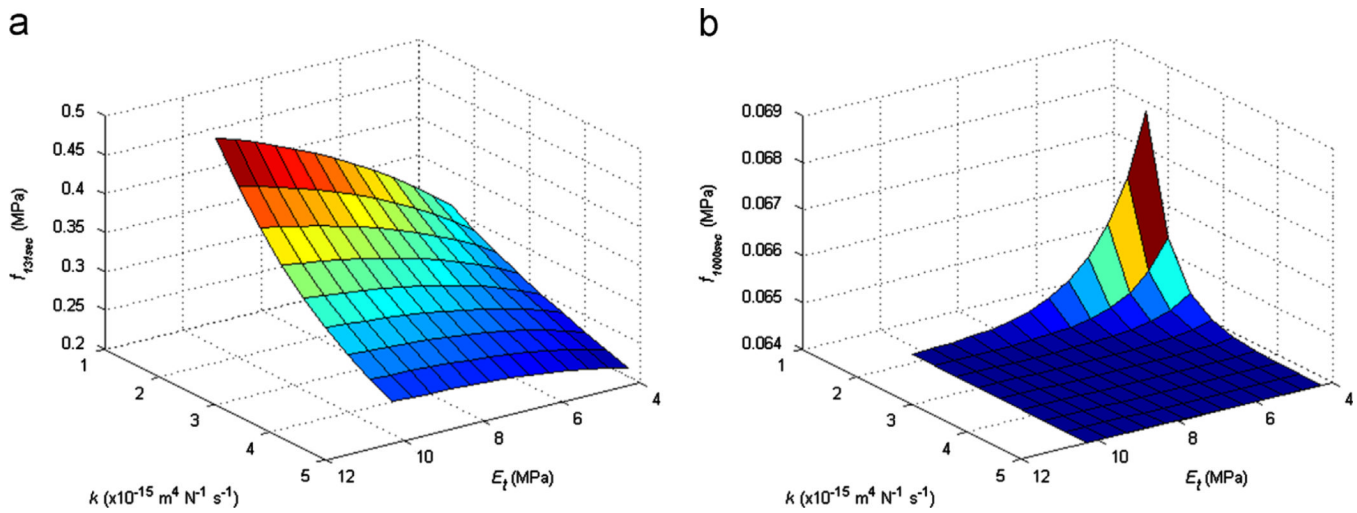

Fig. 8.

Plots of load intensity at (a) 131 s and (b) 1000 s as a function of Young's modulus in plane and permeability where $E_a = 0.64$ MPa, $\nu_t = 0.49$ and $\nu_{at} = 0$.

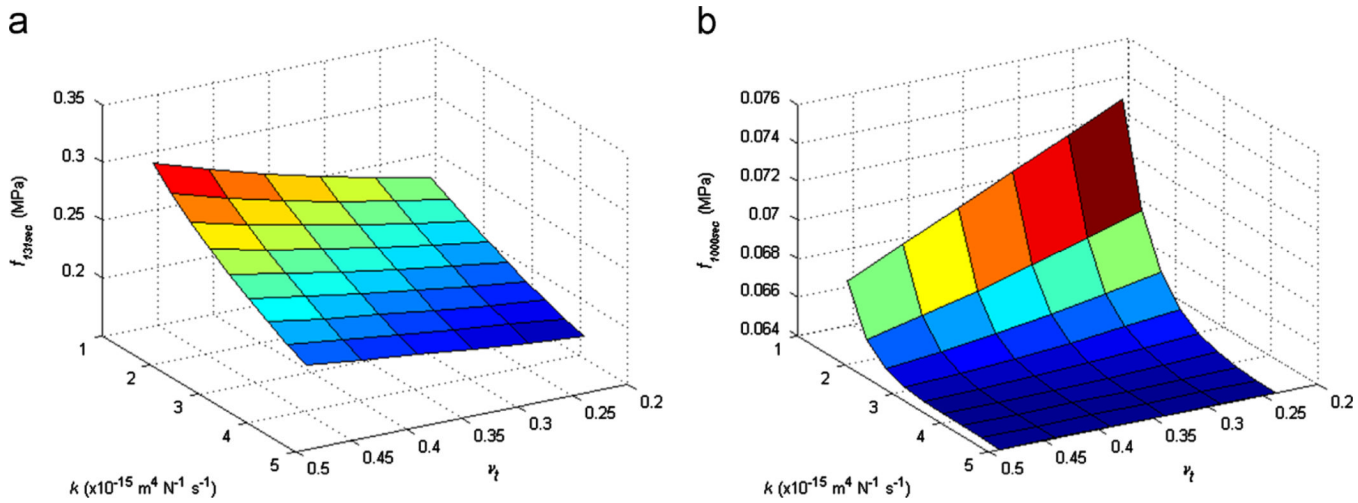

Fig. 9.

Plots of load intensity at (a) 131 s and (b) 1000 s as a function of Poisson's ratio in plane and permeability where E_t = 4.3 MPa, E_a =0.64 MPa and ν_{at} = 0.

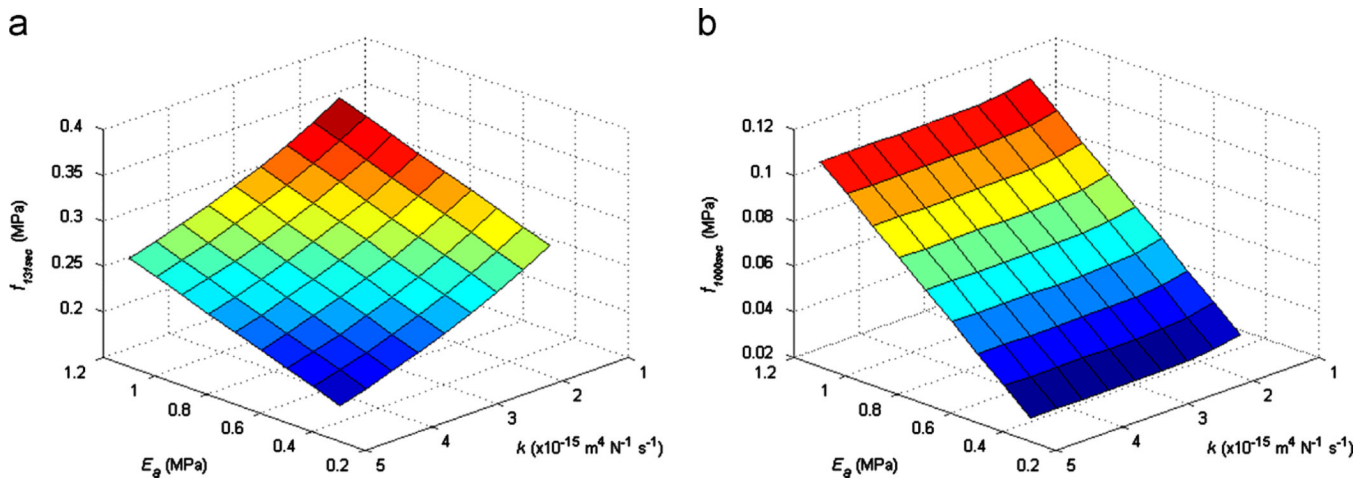

Fig. 10.

Plots of load intensity at (a) 131 s and (b) 1000 s as a function of permeability and Young's modulus out of plane where $E_t = 4.3$ MPa, $\nu_t = 0.49$ and $\nu_{at} = 0$.

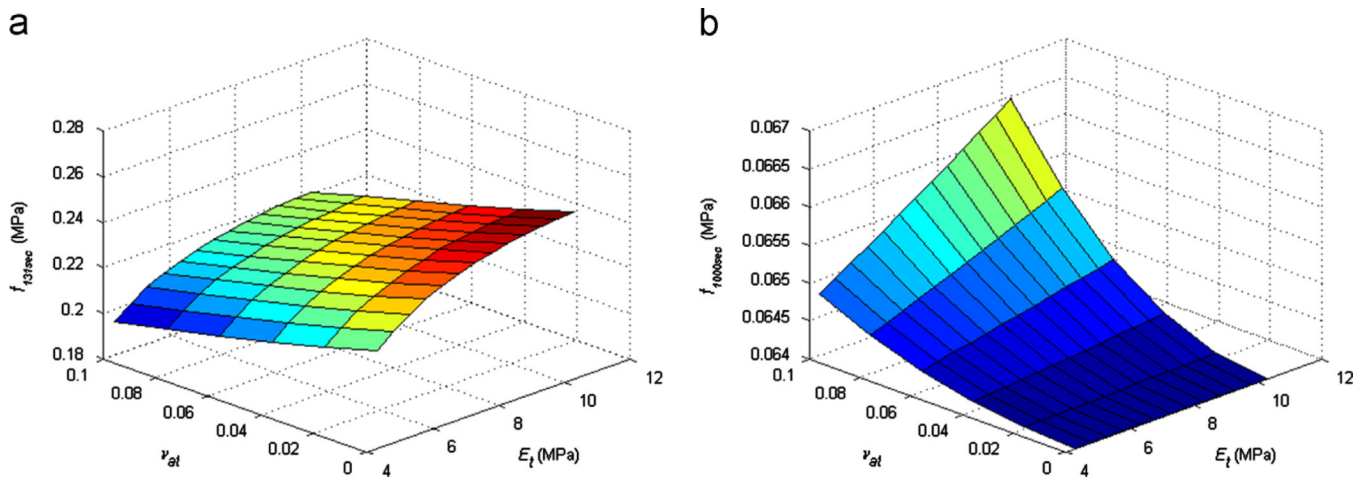

Fig. 11.

Plots of load intensity at (a) 131 s and (b) 1000 s as a function of Young's modulus in plane and Poisson's ratio out of plane where $E_a = 0.64$ MPa, $\nu_t = 0.49$ and $k = 5 \times 10^{-15}$ m^4 N^{-1} s^{-1}.

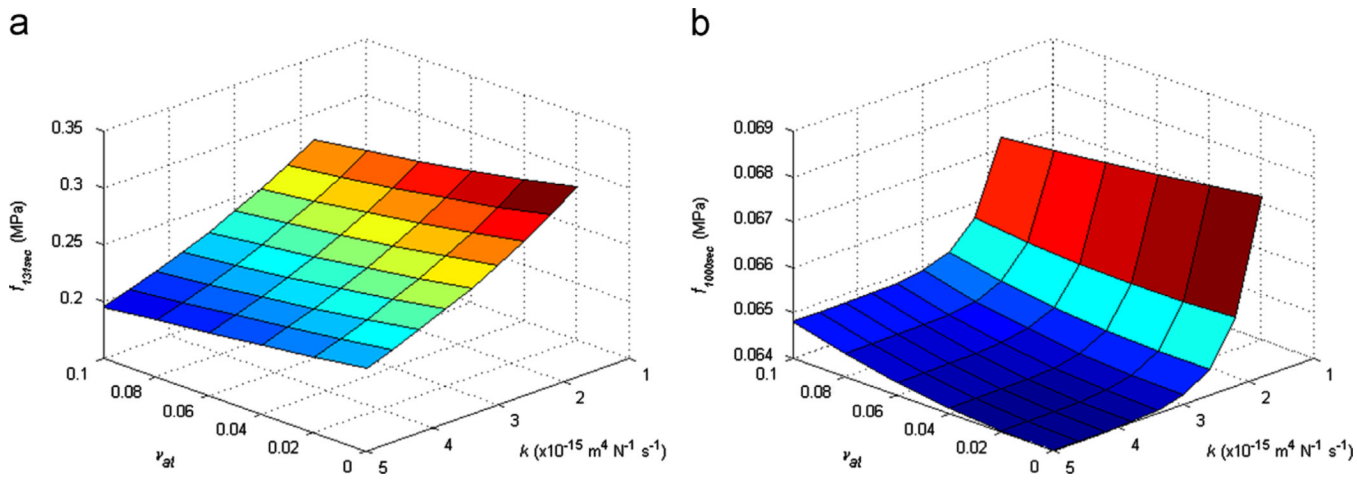

Fig. 12.

Plots of load intensity at (a) 131 s and (b) 1000 s as a function of permeability and Poisson's ratio out of plane where $E_t = 4.3$ MPa, $E_a = 0.64$ MPa and $\nu_t = 0.49$.

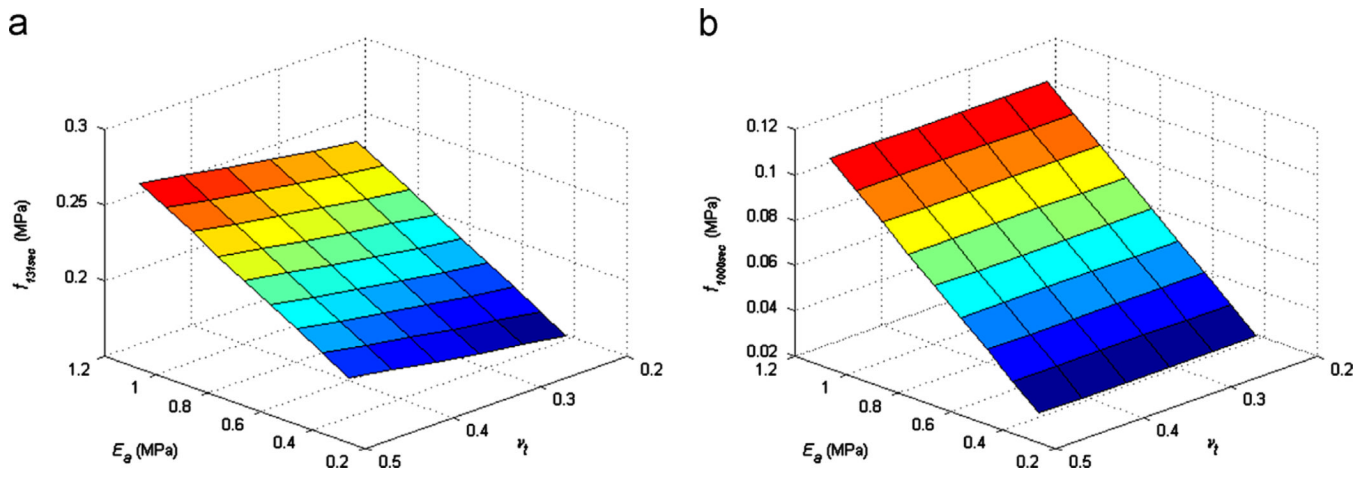

Fig. 13.

Plots of load intensity at (a) 131 s and (b) 1000 s as a function of Young's modulus out of plane and Poisson's ratio in plane where $E_t = 4.3$ MPa, $\nu_{at} = 0$ and $k = 5 \times 10^{-15}$ m^4 N^{-1} s^{-1}.

Table 1

Values of material properties used to simulate stress relaxation in the transversely isotropic finite element model.

Material property	Range
Young's modulus in plane E_t (MPa)	4.3–10.3 in 0.5 increment
Young's modulus out of plane E_a (MPa)	0.3–1.1 in 0.1 increment
Poisson's ratio in transverse plane ν_t	0.24–0.49 in 0.05 increment
Poisson's ratio out of plane ν_{at}	0–0.1 in 0.02 increment
Permeability k ($\times 10^{-15}$ m^4 N^{-1} s^{-1})	1.8–5.0 in 0.4 increment

Table 2

Predicted percentage error of material properties for combinations of five regression equations at different time points during stress relaxation and the corresponding value of ν_{at}.

Time points (s)	E_t (%)	E_a (%)	ν_t (%)	k (%)	ν_{at}
131, 205, 304, 390, 500	13.4	1.42	13.1	2.03	0.0014
131, 205, 304, 390, 619	11.6	1.09	10.9	1.99	−0.0007
131, 205, 304, 390, 700	10.5	0.897	9.56	1.97	−0.0019
131, 205, 304, 390, 800	9.64	0.737	8.47	1.95	−0.0029
131, 205, 304, 390, 1000	8.16	0.467	6.61	1.91	−0.0046